

# An Algorithm to Compute the X-ray Transform

*Chong Chen\** and *Runqian Wang†*

## Abstract

The X-ray transform models a forward projection operator of image formation, which has been widely used for tomographic image reconstruction. We propose a new algorithm to compute that transform of an image represented by unit (pixel/voxel) basis functions, for various two-dimensional (2D)/three-dimensional (3D) scanning geometries, such as 2D/3D parallel beam, 2D fan beam, 3D circular/helical cone beam, etc. Since the transform is acting as a line integral, the fundamental task is to calculate this integral of the unit basis functions, which is equivalently the intersection length of the ray with the associated unit. For a given ray, using the support of unit basis function, we derive the sufficient and necessary condition of non-vanishing intersectability, and obtain the analytic formula for the intersection length, which can be used to distinguish the units that produce valid intersections with the given ray, and then perform simple calculations only for those units. The algorithm is easy to be implemented, and the computational cost is optimal. Moreover, we discuss the intrinsic ambiguities of the problem itself that perhaps happen, and present a solution. The algorithm not only possesses the adaptability with regard to the center position, scale and size of the image, and the scanning geometry as well, but also is quite suited to parallelize with optimality. The resulting projection matrix can be sparsely stored and output if needed, and the adjoint of X-ray transform can be also computed by the algorithm. Finally, we validate the correctness of the algorithm by the aforementioned scanning geometries.

**Keywords:** X-ray transform, forward projection matrix, intersection length, intersectability condition, analytic formula, ambiguity and adaptability, tomographic image reconstruction

## 1 Introduction

The tomography is quite critical in clinical diagnosis, such as computed tomography (CT), positron emission tomography (PET), single photon emission computed tomography (SPECT), etc. [17, 7], and in structure biology as well, such as cryo-electron microscopy (Cryo-EM), electron tomography (ET), etc. [11, 12]. The X-ray transform models a forward projection operator of image formation for the above imaging modalities, which has been widely used for

---

\*LSEC, ICMSEC, Academy of Mathematics and Systems Science, Chinese Academy of Sciences, Beijing 100190, China (chench@lsec.cc.ac.cn).

†Princeton International School of Mathematics and Science, Princeton, NJ.

tomographic image reconstruction [26, 12]. To reduce the radiation or conduct fast scanning, the low-dose or sparse-view sampling is often required. However, the conventional analytic methods (filtered/weighted backprojection) for image reconstruction does not work well for this kind of data. Recently, the advanced methods based on regularization, compressed sensing and/or deep learning have been gained extensive study, due to their ability to allow reducing dose or scanning views while maintaining or improving reconstructed image quality (for instance, see [4, 9, 20, 32, 33, 22, 18, 10, 31, 27, 36, 23, 6, 1, 14, 29, 37, 2, 5]).

It is well-known that the most computationally intensive components for each iterate or each layer locates in the computations of X-ray transform and its adjoint [32, 6, 2]. Mathematically, the computation of the adjoint can be converted into calculating X-ray transform. The aim of this work is to investigate the algorithm for computing the X-ray transform.

The X-ray transform is equivalently called one-dimensional (1D) Radon transform [16]. More precisely, the X-ray transform  $\mathcal{P}$  is given as follows: if  $\theta \in \mathbb{S}^{d-1}$  for  $d = 2$  or  $3$ , and  $\mathbf{x} \in \theta^\perp$ , then

$$\mathcal{P}f(\theta, \mathbf{x}) = \int_{-\infty}^{+\infty} f(\mathbf{x} + t\theta) dt. \quad (1)$$

The formula above is actually the integral of function  $f$  over the straight line (ray) through point  $\mathbf{x}$  with direction  $\theta$  [26, 12]. Note that the function  $f$  is the image to be reconstructed, which is often represented by the unit (pixel/voxel) basis functions  $\{b_i\}$  as

$$f(\mathbf{r}) = \sum_i f_i b_i(\mathbf{r}), \quad (2)$$

where  $f_i$  is the given gray value of the  $i$ -th unit, and

$$b_i(\mathbf{r}) = \begin{cases} 1, & \mathbf{r} \in \Omega_i, \\ 0, & \text{otherwise.} \end{cases}$$

Here  $\Omega_i \subset \mathbb{R}^d$  is the  $i$ -th unit of the image. By (1) and (2), the X-ray transform of the image function can be written as

$$\mathcal{P}f(\theta, \mathbf{x}) = \sum_i f_i \int_{-\infty}^{+\infty} b_i(\mathbf{x} + t\theta) dt, \quad (3)$$

which is to compute the summation of the intersection lengths of the ray with each unit weighted by its gray value. Hence the fundamental problem of (3) is to calculate the line integral of the unit basis functions, which is equivalently the intersection length of the ray with the associated unit. The focus of this article is on studying this problem.

The intersection lengths of a certain ray with all the units construct a row of the forward projection matrix, where its entry is the associated intersection length. Actually, the computation of the X-ray transform of all rays (forward projection) is also equivalent to compute the projection matrix multiplying a vectorized image, and the computation of their adjoints (backprojection) means to compute the transpose of the projection matrix multiplying a corresponding vector. The projection matrix is of particularly interest to develop and validate

the related reconstruction algorithms, which can be stored in sparse pattern if permitted to avoid its repeat calculations during algorithm implementation.

There are several algorithms developed to compute the X-ray transform (see [30, 19, 15, 38, 8, 25, 13, 24]). Some of them compute the intersection lengths inexactly. A classical accurate algorithm was proposed by Siddon in [30], which requires to compute the intersection points of the ray with all of the grid lines/planes in 2D/3D circumstances, and then sorts all those intersection points. Some speedup versions of Siddon’s algorithm were developed in [19, 15, 13]. There are also many software packages that can be used to aid the implementations of the related reconstruction algorithms, for instance, STIR [34], RTK [28], ASTRA [35], TIGRE [3], etc. Many of them calculate the (approximate) X-ray transform and its adjoint following Siddon’s algorithm, and/or perform a few of commonly scanning geometries.

**Contributions.** In this work, the main contribution is that we propose a fast, accurate, adaptive and parallelizable algorithm to compute the X-ray transform of an image represented by unit (pixel/voxel) basis functions, for various 2D/3D scanning geometries, such as 2D/3D parallel beam, 2D fan beam, 3D circular/helical cone beam, etc. This algorithm can be used to assist implementing the iterative or deep learning based reconstruction algorithms for various tomographic imaging arisen in medicine, biology, and industry, to just name a few.

More importantly, we derive the sufficient and necessary condition for non-vanishing intersectability, and obtain the analytic formula for the intersection length, which can be used to distinguish the units that produce valid intersections with the given ray, and then perform simple calculations only for those units. Based on the results above, the algorithm becomes quite easy to be implemented, and its computational cost is optimal.

We further discuss the intrinsic ambiguities of the problem itself that perhaps happen, and give a solution in the algorithm. Moreover, the algorithm not only possesses the adaptability with regard to the center position, scale and size of the image, and the scanning geometry as well, but also is quite suited to parallelize with optimality. The projection matrix can be sparsely stored and output if needed, and the adjoint of X-ray transform can be also computed by the algorithm. Hence, the algorithm can be customized freely according to the requirements of the users, and more scanning geometries can be easily added into the framework based on the proposed algorithm.

**Outline.** The algorithms for various 2D and 3D scanning geometries are proposed in section 2 and section 3, respectively. Section 4 points out the intrinsic ambiguities of the problem itself, and presents a solution accordingly, and also includes the discussions on the adaptability and parallelization of the proposed algorithm. The validations are performed in section 5. Finally, section 6 concludes the paper.

## 2 Algorithm for 2D scanning geometries

The purpose of this section is to develop the algorithm for 2D scanning geometries. To begin with, we need to introduce several requisite preliminaries.

## 2.1 Preliminaries

Here we present some preliminaries, including the commonly used 2D scanning geometries, 2D imaging coordinate system, and pixel indexes.

**2D scanning geometries.** For 2D case, there are normally two scanning geometries at which the rays are distributed, namely, parallel beam and fan beam (including equiangular and equispaced) [21, 17]. Parallel beam, as its name suggested, stands for a group of parallel X-rays penetrating through the detected object, as shown in fig. 1. Fan beam, on the other hand, is a set of beams emitted from one source point, and gets detected from a series of detectors, as shown in fig. 2. When the detectors are placed such that the angles between any two consecutive rays are equal, it is called equiangular fan beam; When the detectors are aligned with equal space between any two adjacent detectors, it is named equispaced fan beam.

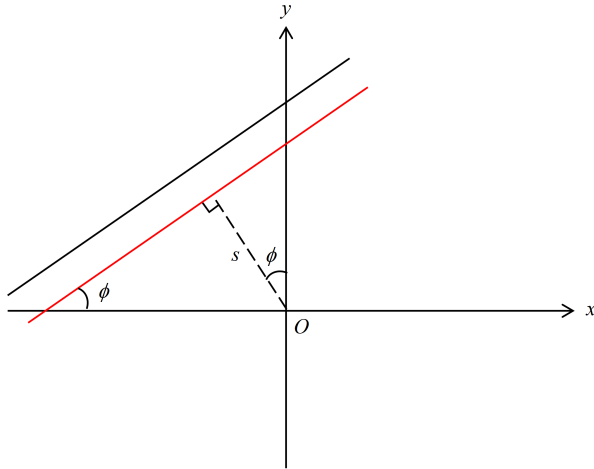


Fig. 1: 2D parallel beam

**2D imaging coordinate system.** Let  $(x, y)$  be the coordinate system. For a image to be reconstructed, we assume that the parameters  $L_x$ ,  $L_y$ , and  $N_x$ ,  $N_y$  are given, where  $(L_x, L_y)$  and  $(N_x, N_y)$  specify the side lengths of the domain and the size of the image along  $x$ - and  $y$ -axis, respectively. Let  $(d_x, d_y) := (L_x/N_x, L_y/N_y)$  be the side lengths or scales of the pixel along  $x$ - and  $y$ -axis. Without loss of generality, we assume that  $L_x = L_y$ ,  $N_x = N_y$ , accordingly,  $d_x = d_y$ , and the center of the image domain is at the origin  $O$  of the coordinate system as shown in fig. 3. For simplicity, we further assume that the scale  $d_x = d_y = 1$ . If the scale is not unity, the real value of X-ray transform just equals to the scale multiplying that value for the case with unity scale.

**Pixel indexes.** We define two different indexes for the pixels of the image. The one is given in 1D form as  $I = 0, 1, \dots, N_x N_y - 1$ , which is shown as the example with  $N_x = N_y = 7$  in fig. 3. The other one is presented in 2D form as  $(j, i)$  with  $j = 0, 1, \dots, N_y - 1$ ,  $i = 0, 1, \dots, N_x - 1$ , which is shown as the example also

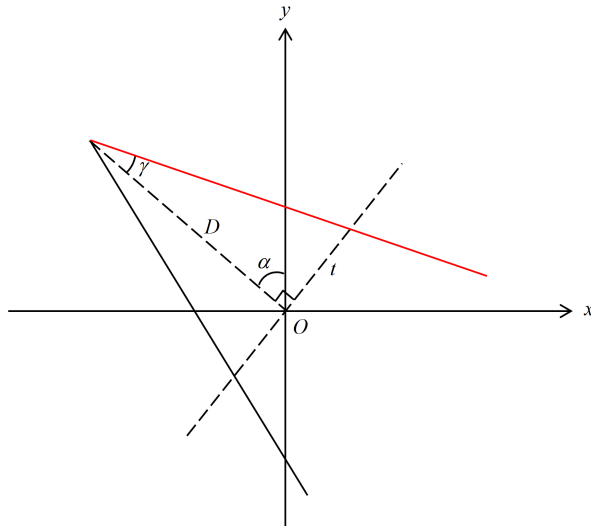


Fig. 2: Fan beam

with  $N_x = N_y = 7$  in fig. 4. The relation between them can be expressed as  $I = jN_y + i$ , which can be easily validated by the examples in fig. 3 and fig. 4. They are able to convert into each other.

Here the first and the second indexes are used to indicate the pixel positions in the associated vectorized image and the original image, respectively. They are independent of the coordinate system. The first one is used in sparse storage of projection matrix in numerical implementation of this paper. Note that the second one is different from the coordinate position of the pixel. Later in computation, when referring to any location of the pixel/voxel, we will use its indexes rather than coordinate position. The coordinate positions are only used in the implementation of the algorithm.

In this section, we will use pixel  $(j, i)$  to indicate the pixel with index  $(j, i)$ . The valid  $j$  (or  $i$ ) is for itself satisfying  $0 \leq j \leq N_y - 1$  (or  $0 \leq i \leq N_x - 1$ ).

## 2.2 Derivation of intersection length

Here we will give the mathematical derivations of intersection length for various 2D scanning geometries.

### 2.2.1 2D parallel beam

To calculate the intersection length, the position of the ray and the pixel need to be determined. Assuming that the parameters  $s \in \mathbb{R}^1$  and  $\phi \in [0, \pi)$  are given, where the  $(s, \phi)$  determines a ray of the parallel beam in 2D plane as shown in fig. 1. More precisely, the  $s$  is the signed distance between the ray and the origin, and the  $\phi$  is the angle between the ray and the positive  $x$ -axis.

Given ray  $(s, \phi)$ , the resulting unit direction and normal of the ray are

$$\theta = (\cos \phi, \sin \phi) \quad \text{and} \quad \theta^\perp = (-\sin \phi, \cos \phi), \quad (4)$$

respectively.

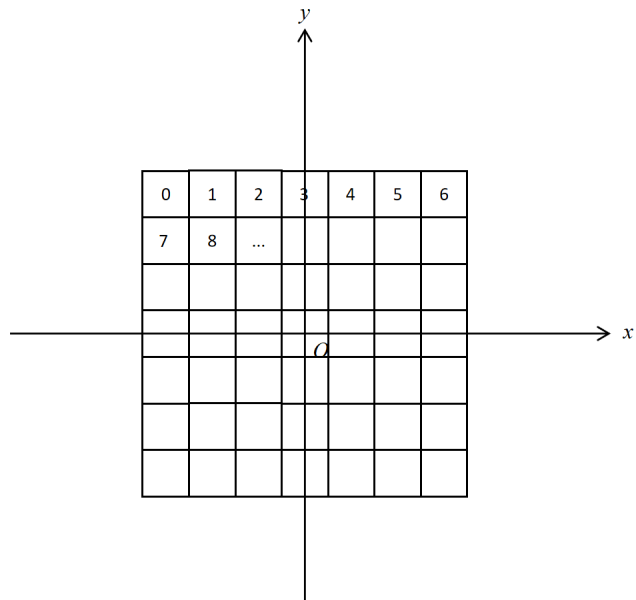


Fig. 3: Pixel index in 1D form

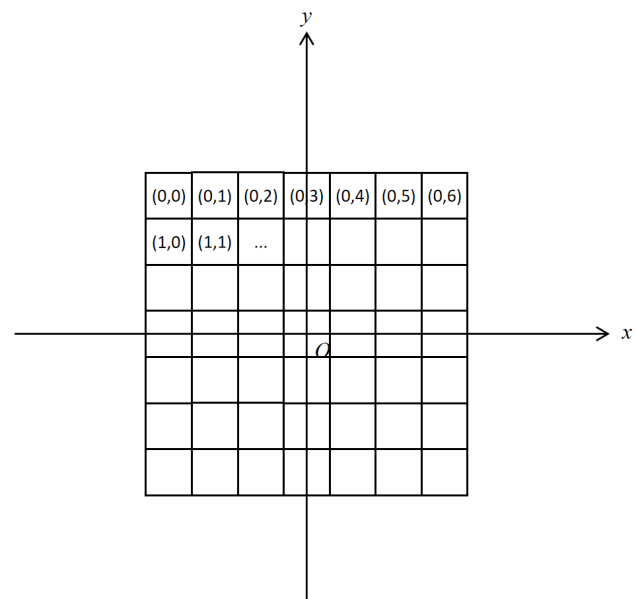


Fig. 4: Pixel index in 2D form

As assumed in the above, the scale  $d_x = d_y = 1$ . We then give the transformational relation between the 2D-form index of the pixel and the coordinate position of its center. For any pixel with index  $(j, i)$ , its center is located at the coordinate position

$$\left( i - \frac{N_x - 1}{2}, \frac{N_y - 1}{2} - j \right).$$

Hence the associated pixel basis function is defined as

$$f_{ji}(x, y) = \begin{cases} 1, & (x, y) \in \Omega_{ji}, \\ 0, & \text{otherwise,} \end{cases} \quad (5)$$

where  $\Omega_{ji} := [i - \frac{N_x}{2}, i - \frac{N_x}{2} + 1] \times [\frac{N_y}{2} - j - 1, \frac{N_y}{2} - j]$  denotes the support of pixel  $(j, i)$ .

The intersection length  $l_{ji}(s, \phi)$  between the ray  $(s, \phi)$  and pixel  $(j, i)$  can be expressed as the X-ray transform of the associated pixel basis function, namely,

$$l_{ji}(s, \phi) = \int_{-\infty}^{\infty} f_{ji}(t\theta + s\theta^{\perp}) dt. \quad (6)$$

Using (4) and (5), the (6) implies that if and only if the following condition is satisfied

$$\begin{cases} i - \frac{N_x}{2} \leq t \cos \phi - s \sin \phi \leq i - \frac{N_x}{2} + 1, \\ \frac{N_y}{2} - j - 1 \leq t \sin \phi + s \cos \phi \leq \frac{N_y}{2} - j, \end{cases} \quad (7)$$

then the length of intersection might be nonzero. Note that the variable  $t$  of integration in (6) is along the ray. Therefore, the range of  $t$  that satisfies the inequalities in (7) would be the length of intersection.

As observed, the ray  $(s, \phi + 2n\pi)$  for  $n \in \mathbb{Z}$  is equivalent to the ray  $(s, \phi)$ , and the ray  $(s, \phi + \pi)$  is just the same as the ray  $(-s, \phi)$ . Hence any ray can be determined by the ray  $(s, \phi) \in \mathbb{R}^1 \times [0, \pi)$ . In what follows we list the cases by the choice of  $\phi$ .

**Case 1:**  $\phi \in (0, \pi/2)$ . For simplicity, let

$$\begin{cases} C_x = \frac{i - N_x/2 + s \sin \phi}{\cos \phi}, \\ C_y = \frac{N_y/2 - j - s \cos \phi}{\sin \phi}. \end{cases} \quad (8)$$

Using simple calculations, by (8), the (7) can be translated into

$$\begin{cases} C_x \leq t \leq C_x + \frac{1}{\cos \phi}, \\ C_y - \frac{1}{\sin \phi} \leq t \leq C_y. \end{cases} \quad (9)$$

As we observed, if the two intervals in (9) are disjointed or their overlap is just a point, then the length of the intersection is definitely vanishing. To exclude this possibility, if and only if

$$C_{low} < C_{up}, \quad (10)$$

where

$$C_{low} = \max(C_x, C_y - 1/\sin \phi), \quad C_{up} = \min(C_x + 1/\cos \phi, C_y).$$

Evidently, (10) is equivalent to

$$\begin{cases} C_x < C_y, \\ C_y - \frac{1}{\sin \phi} < C_x + \frac{1}{\cos \phi}. \end{cases} \quad (11)$$

The (10) or (11) is just the *sufficient and necessary condition* for non-vanishing intersectability of the given ray and pixel. More precisely, the *non-vanishing intersectability* means the length of the intersection being non-vanishing.

More specifically, by (8), if the  $i$  is given, the condition (11) is equivalent to the following inequality

$$C_1 - \tan \phi - 1 < j < C_1, \quad (12)$$

where

$$C_1 = \frac{N_y}{2} - s \cos \phi - C_x \sin \phi.$$

Similarly, provided that the  $j$  is given, the condition (11) can be rewritten as

$$C_2 - \cot \phi - 1 < i < C_2, \quad (13)$$

where

$$C_2 = \frac{N_x}{2} - s \sin \phi + C_y \cos \phi.$$

Hence, for any given  $i$  or  $j$ , we can calculate the range of valid  $j$  by (12), or that of valid  $i$  by (13), to obtain those pixels intersecting with the given ray non-vanishingly. For those pixels, the condition (10) is surely satisfied. By merging the intervals in (9), we get the intersection as

$$C_{low} \leq t \leq C_{up}. \quad (14)$$

Otherwise, the intersection is empty. Hence, the *analytic formula* of the intersection length should be

$$l_{ji}(s, \phi) = \max(0, C_{up} - C_{low}). \quad (15)$$

**Case 2:**  $\phi = 0$ . The (7) becomes

$$\begin{cases} i - \frac{N_x}{2} \leq t \leq i - \frac{N_x}{2} + 1, \\ \frac{N_y}{2} - j - 1 \leq s \leq \frac{N_y}{2} - j. \end{cases} \quad (16)$$

Obviously, for any given  $i$ , if the valid  $j$  is satisfying  $\frac{N_y}{2} - s - 1 \leq j \leq \frac{N_y}{2} - s$ , the intersection length is unity, otherwise, it is zero.

*Remark 1.* For the case  $\phi \in (\pi/2, \pi)$ , the corresponding sufficient and necessary condition for non-vanishing intersectability, and analytic formula of the intersection length can be easily obtained by making quite slight changes to the derivation in the above **case 1**.

Similarly, the intersection length can be immediately calculated for the case  $\phi = \pi/2$  by the method of **case 2**. Note that the rays in such cases are parallel to a certain axis, which results in quite simple calculations, but the ambiguity perhaps happen (see the first example in section 4.1).

To summarize, the proposed algorithm is optimized to  $O(N)$  for any given ray, and  $O(NM)$  for all rays, where  $N$  stands for the size of the image being reconstructed along one axis, and  $M$  denotes the number of rays. Hence, this algorithm has achieved to the degree of optimality.

### 2.2.2 Fan beam

Apart from the 2D parallel beam, as mentioned previously, the fan beam is often used in 2D circumstance. Therefore, the algorithm should be able to adapt to this situation.

**Equiangular fan beam.** The second pattern is equiangular fan beam as shown in fig. 2. Essentially, any ray of the equiangular fan beam can be determined by the parameters  $(D, \alpha, \gamma)$ , where  $D > 0$  indicates the distance of source for X-rays from the origin  $O$ ,  $\alpha \in [0, 2\pi)$  stands for the angle between the line from the origin to source and the positive  $y$ -axis, and  $\gamma \in [-\gamma_m, \gamma_m]$  specifies the signed angle between the line from the source to the origin and each ray. The radian  $\gamma_m \in (0, \pi/2)$  determines the size of the view field for fan beam.

Then the aim is to find the corresponding parameters  $(s, \phi)$  in 2D parallel beam for each ray when given  $(D, \alpha, \gamma)$ , as indicated in fig. 2. In this case, it is quite straightforward:

$$\begin{cases} s = D \sin \gamma, \\ \phi = \gamma + \alpha - \frac{\pi}{2}. \end{cases} \quad (17)$$

The above transformation can be also referred to [21]. After transformation, the associated X-ray transform can be readily computed by the algorithm developed in section 2.2.1.

**Equispaced fan beam.** As shown in fig. 2, the equispaced fan beam is quite similar with the equiangular one. But the one given parameter is about the signed distance along the line corresponding to the detector bank [21]. In other words, the given parameter is  $t \in [-t_m, t_m]$  compared to the  $\gamma$  in the previous case. Here the  $t_m > 0$  determines the size of the view field for fan beam. Thus, for each ray with the given parameters  $(D, \alpha, t)$ , in what follows we only need to perform several minor changes to the derivation above

$$\begin{cases} s = \frac{Dt}{\sqrt{D^2+t^2}}, \\ \phi = \arctan\left(\frac{t}{D}\right) + \alpha - \frac{\pi}{2}. \end{cases} \quad (18)$$

Similarly, the associated X-ray transform in equispaced fan beam can be computed by the algorithm developed in section 2.2.1.

## 3 Algorithm for 3D scanning geometries

Here the aim is to further develop the algorithm for 3D scanning geometries. To proceed, we first introduce some preliminaries.

### 3.1 Preliminaries

The purpose of this part is to state some requisite preliminaries for 3D case, including the often used 3D scanning geometries, 3D imaging coordinate system, voxel indexes, and Eulerian angles.

**3D scanning geometries.** In 3D circumstance, there are three patterns commonly used, including parallel beam, circular cone beam and helical cone beam [21, 12, 17]. The 3D Parallel beam is almost the same as in 2D situation, where all beams from one view are parallel to each other, as shown in fig. 5. Apart

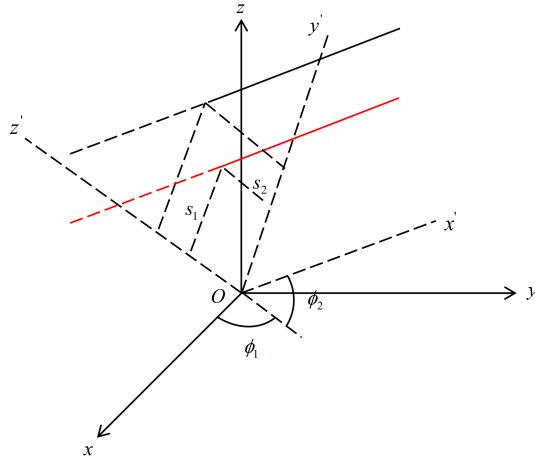


Fig. 5: 3D parallel beam

from the applications in medical imaging, such beam has been widely applied in biological imaging (e.g., Cryo-EM and ET) [12, 11]. Circular cone beam can be seen as the extension of the fan beam, where the X-ray source is performing uniformly circular motion around the rotating axis, as shown in fig. 6. This beam naturally includes the equiangular and equispaced patterns. Helical cone beam is often used when scanning through a long object, where the X-ray source relatively moves with constant speed along one axis while performing uniformly circular motion on the perpendicular plane [17], as shown in fig. 7.

**3D imaging coordinate system.** Let  $(x, y, z)$  be the coordinate system. For a scanning 3D image, supposing that the positive parameters  $L_x, L_y, L_z$  and  $N_x, N_y, N_z$  are given, where  $(L_x, L_y, L_z)$  and  $(N_x, N_y, N_z)$  determine the side lengths of the domain and the size of the image along  $x$ -,  $y$ - and  $z$ -axis, respectively. Let  $(d_x, d_y, d_z) := (L_x/N_x, L_y/N_y, L_z/N_z)$  be the side lengths or scales of the voxel along the corresponding axes. Without loss of generality, we assume that  $L_x = L_y = L_z, N_x = N_y = N_z$ , accordingly,  $d_x = d_y = d_z$ , and the center of the image domain is at the origin of the coordinate system as shown in fig. 8. For simplicity, we further assume that the scales  $d_x = d_y = d_z = 1$ . If the scale is not unity, the real value of X-ray transform just equals to the scale multiplying that value for the case with unity scale.

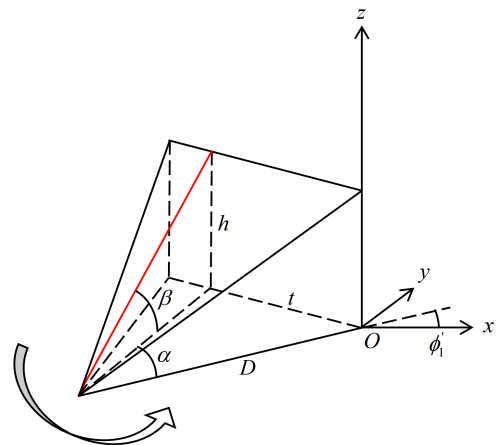


Fig. 6: Circular cone beam

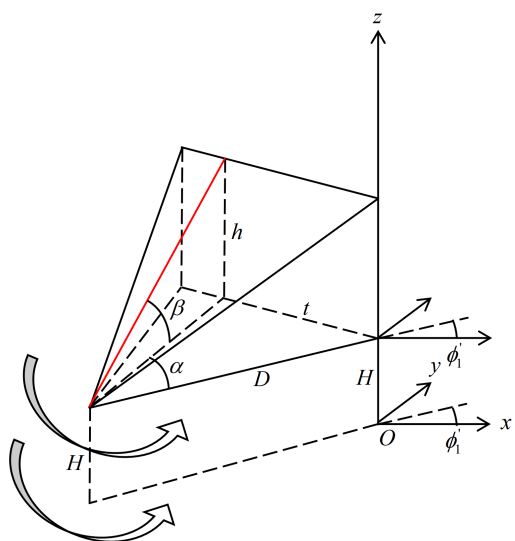


Fig. 7: Helical cone beam

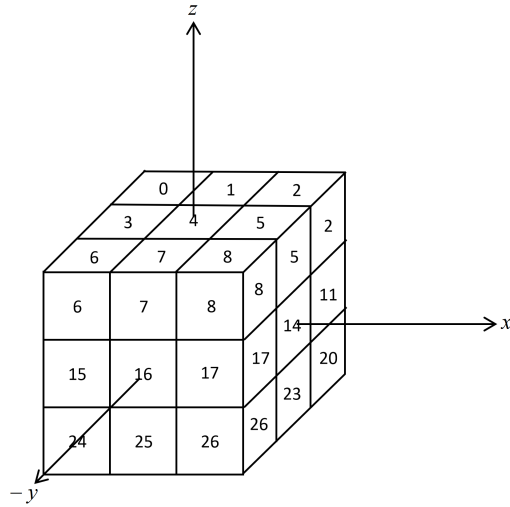


Fig. 8: Voxel index in 1D form

**Voxel indexes.** We also define two different indexes for the voxels of the image. The one is given in 1D form as  $I = 0, 1, \dots, N_x N_y N_z - 1$ , which is shown as the example with  $N_x = N_y = N_z = 3$  in fig. 8. The other one is presented in 3D form as  $(k, j, i)$  for  $k = 0, 1, \dots, N_z - 1$ ,  $j = 0, 1, \dots, N_y - 1$ ,  $i = 0, 1, \dots, N_x - 1$ , which is shown as the example also with  $N_x = N_y = N_z = 3$  in fig. 9. The relation between them can be expressed as  $I = kN_y N_x + jN_y + i$ , which can be easily validated by the examples in fig. 8 and fig. 9. They also can convert between each other.

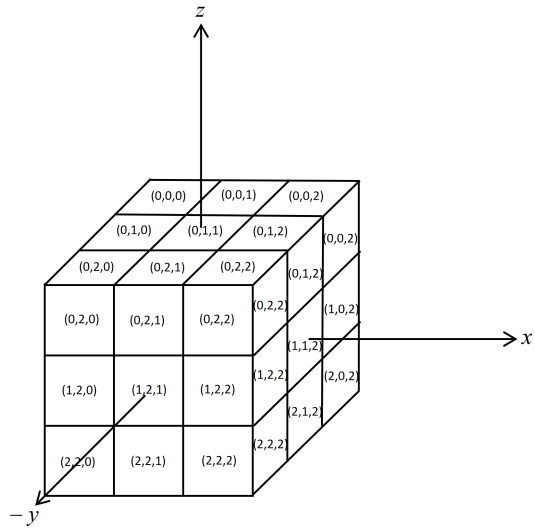


Fig. 9: Voxel index in 3D form

Here the first and the second indexes are used to indicate the voxel positions in the associated vectorized image and the original image, respectively. Note

that the second one is different from the coordinate position of the voxel.

In this section, we will use voxel  $(k, j, i)$  to indicate the voxel with index  $(k, j, i)$ . The valid  $k$  (or  $j, i$ ) is for itself satisfying  $0 \leq k \leq N_z - 1$  (or  $0 \leq j \leq N_y - 1, 0 \leq i \leq N_x - 1$ ).

**Eulerian angles.** To specify an arbitrary ray in 3D case, we need to use the concept of *Eulerian angles* (see [12, Chapter 5]). Assuming that  $(x, y, z)$  is the original coordinate system. If the direction of a ray is  $\theta$ , defined by the three Eulerian angles  $\phi_1, \phi_2$  and  $\phi_3$ , a projection is acquired on the plane that is perpendicular to the ray and also containing the origin. Then a new coordinate system is constructed by the above direction and plane, which is denoted by  $(x', y', z')$  coordinate system. The transformation between the vectors in  $(x, y, z)$  coordinate system and those in  $(x', y', z')$  coordinate system is given by three Eulerian rotations as

$$\begin{bmatrix} x' \\ y' \\ z' \end{bmatrix} = \mathcal{R} \begin{bmatrix} x \\ y \\ z \end{bmatrix}, \quad (19)$$

where

$$\mathcal{R} = \begin{bmatrix} \cos \phi_3 & \sin \phi_3 & 0 \\ -\sin \phi_3 & \cos \phi_3 & 0 \\ 0 & 0 & 1 \end{bmatrix} \begin{bmatrix} \cos \phi_2 & 0 & \sin \phi_2 \\ 0 & 1 & 0 \\ -\sin \phi_2 & 0 & \cos \phi_2 \end{bmatrix} \begin{bmatrix} \cos \phi_1 & \sin \phi_1 & 0 \\ -\sin \phi_1 & \cos \phi_1 & 0 \\ 0 & 0 & 1 \end{bmatrix}.$$

These rotations can be illuminated as that first the  $(x, y, z)$  coordinate system is contra-rotated by the angle  $\phi_1$  around its  $z$ -axis, resulting in the intermediate coordinate system  $(x_1, y_1, z_1)$ , then by the angle  $\phi_2$  around its new  $y$ -axis, yielding the second intermediate coordinate system  $(x_2, y_2, z_2)$ , and finally by the angle  $\phi_3$  around its new  $z$ -axis to lead the final coordinate system  $(x', y', z')$ .

## 3.2 Derivation of intersection length

The purpose of this section is to derive intersection length for various 3D scanning geometries.

### 3.2.1 3D parallel beam

To characterize the 3D parallel beam, we can use the Eulerian angles above. Given that  $(x, y, z)$  is the coordinate system affixed to the image to be reconstructed. By projecting the image along a direction  $\theta$ , a 2D projection is acquired on its perpendicular plane containing the origin. Since the last rotation in (19) is an in-plane rotation, the parallel-beam scanning geometry can be generated by letting  $\phi_3 = 0$ . Then the transformation (19) becomes

$$\begin{bmatrix} x' \\ y' \\ z' \end{bmatrix} = \begin{bmatrix} \cos \phi_2 \cos \phi_1 & \cos \phi_2 \sin \phi_1 & \sin \phi_2 \\ -\sin \phi_1 & \cos \phi_1 & 0 \\ -\sin \phi_2 \cos \phi_1 & -\sin \phi_2 \sin \phi_1 & \cos \phi_2 \end{bmatrix} \begin{bmatrix} x \\ y \\ z \end{bmatrix}. \quad (20)$$

Hence the direction of the parallel beam can be expressed as

$$\theta = (\cos \phi_2 \cos \phi_1, \cos \phi_2 \sin \phi_1, \sin \phi_2), \quad (21)$$

and the associated orthogonal projection plane can be spanned by  $\{\theta_1, \theta_2\}$ , where

$$\theta_1 = (-\sin \phi_1, \cos \phi_1, 0), \quad (22)$$

$$\theta_2 = (-\sin \phi_2 \cos \phi_1, -\sin \phi_2 \sin \phi_1, \cos \phi_2). \quad (23)$$

For the purpose of calculating the intersection length, the position of the ray and the pixel need to be specified. Assuming that the parameters  $s_1, s_2 \in \mathbb{R}^1$  and  $\phi_1 \in [0, 2\pi)$ ,  $\phi_2 \in [0, \pi)$  are given, where the  $(s_1, s_2, \phi_1, \phi_2)$  determines a ray of the parallel beam in 3D space as shown in fig. 5. Specifically, the  $(s_1, s_2)$  is the coordinate position of the ray projecting onto the plane  $\{\theta_1, \theta_2\}$ , and the  $(\phi_1, \phi_2)$  is the Eulerian angles indicating the direction  $\theta$  of the ray.

As assumed, the scales  $d_x = d_y = d_z = 1$ . We then give the transformation between the index of the voxel and the coordinate position of its center. For any voxel with index  $(k, j, i)$ , its center is located at the coordinate position

$$\left( i - \frac{N_x - 1}{2}, \frac{N_y - 1}{2} - j, \frac{N_z - 1}{2} - k \right).$$

The associated voxel basis function is defined as

$$f_{kji}(x, y, z) = \begin{cases} 1, & (x, y, z) \in \Omega_{kji}, \\ 0, & \text{otherwise.} \end{cases} \quad (24)$$

where  $\Omega_{kji} := [i - \frac{N_x}{2}, i - \frac{N_x}{2} + 1] \times [\frac{N_y}{2} - j - 1, \frac{N_y}{2} - j] \times [\frac{N_z}{2} - k - 1, \frac{N_z}{2} - k]$  denotes the support of voxel  $(k, j, i)$ .

The intersection length  $l_{kji}(s_1, s_2, \phi_1, \phi_2)$  between the ray  $(s_1, s_2, \phi_1, \phi_2)$  and the voxel  $(k, j, i)$  can be expressed as the X-ray transform of the associated voxel basis function by

$$l_{kji}(s_1, s_2, \phi_1, \phi_2) = \int_{-\infty}^{\infty} f_{kji}(t\theta + s_1\theta_1 + s_2\theta_2) dt. \quad (25)$$

By (21)-(24), the (25) implies that if and only if the following condition is satisfied

$$\begin{cases} i - \frac{N_x}{2} \leq t \cos \phi_2 \cos \phi_1 - s_1 \sin \phi_1 - s_2 \sin \phi_2 \cos \phi_1 \leq i - \frac{N_x}{2} + 1, \\ \frac{N_y}{2} - j - 1 \leq t \cos \phi_2 \sin \phi_1 + s_1 \cos \phi_1 - s_2 \sin \phi_2 \sin \phi_1 \leq \frac{N_y}{2} - j, \\ \frac{N_z}{2} - k - 1 \leq t \sin \phi_2 + s_2 \cos \phi_2 \leq \frac{N_z}{2} - k, \end{cases} \quad (26)$$

then the length of intersection might be non-vanishing. Note that the variable  $t$  of integration in (25) is along the ray. Therefore, the range of  $t$  that satisfies the inequalities in (26) would be the length of intersection.

As we observe, the ray  $(s_1, s_2, \phi_1 + 2n_1\pi, \phi_2 + 2n_2\pi)$  for  $n_1, n_2 \in \mathbb{Z}$  is equivalent to the ray  $(s_1, s_2, \phi_1, \phi_2)$ , the ray  $(s_1, s_2, \phi_1, \phi_2 + \pi)$  is the same as the ray  $(s_1, -s_2, \phi_1, \phi_2)$ , and the ray  $(-s_1, s_2, \phi_1 + \pi, -\phi_2)$  is the same as the ray  $(s_1, s_2, \phi_1, \phi_2)$ . Note that if  $(\phi_1, \phi_2) \in [0, 2\pi) \times \{\pi/2\}$ , the direction of the associated rays are the same, i.e., the positive  $z$ -axis. Hence this kind of rays can be reduced to the ray  $\mathbb{R}^1 \times \mathbb{R}^1 \times \{0\} \times \{\pi/2\}$ . Conclusively, any ray can be specified by the ray  $(s_1, s_2, \phi_1, \phi_2) \in \{\mathbb{R}^1 \times \mathbb{R}^1 \times [0, 2\pi) \times [0, \pi/2]\} \cup \{\mathbb{R}^1 \times \mathbb{R}^1 \times \{0\} \times \{\pi/2\}\}$ . By the analysis above, the possible cases has been largely reduced. In what follows we list the cases by the different choices of  $(\phi_1, \phi_2)$ .

**Case 1:**  $(\phi_1, \phi_2) \in (0, \pi/2) \times (0, \pi/2)$ . For simplicity, let

$$\begin{cases} C_x = \frac{i - N_x/2 + s_1 \sin \phi_1 + s_2 \sin \phi_2 \cos \phi_1}{\cos \phi_2 \cos \phi_1}, \\ C_y = \frac{N_y/2 - j - s_1 \cos \phi_1 + s_2 \sin \phi_2 \sin \phi_1}{\cos \phi_2 \sin \phi_1}, \\ C_z = \frac{N_z/2 - k - s_2 \cos \phi_2}{\sin \phi_2}. \end{cases} \quad (27)$$

By simple calculations, using (27), the condition (26) becomes

$$\begin{cases} C_x \leq t \leq C_x + \frac{1}{\cos \phi_2 \cos \phi_1}, \\ C_y - \frac{1}{\cos \phi_2 \sin \phi_1} \leq t \leq C_y, \\ C_z - \frac{1}{\sin \phi_2} \leq t \leq C_z. \end{cases} \quad (28)$$

Obviously, if the three intervals in (28) have no overlap or their overlap is just a point, then the length of the intersection is absolutely zero. To rule out this possibility, if and only if

$$C_{low} < C_{up}. \quad (29)$$

Here

$$\begin{aligned} C_{low} &= \max(C_x, C_y - 1/(\cos \phi_2 \sin \phi_1), C_z - 1/\sin \phi_2), \\ C_{up} &= \min(C_x + 1/(\cos \phi_2 \cos \phi_1), C_y, C_z). \end{aligned}$$

Equivalently, (29) can be rewritten as

$$\begin{cases} C_x < C_y, \\ C_y - \frac{1}{\cos \phi_2 \sin \phi_1} < C_x + \frac{1}{\cos \phi_2 \cos \phi_1}, \\ C_x < C_z, \\ C_z - \frac{1}{\sin \phi_2} < C_x + \frac{1}{\cos \phi_2 \cos \phi_1}, \\ C_y - \frac{1}{\cos \phi_2 \sin \phi_1} < C_z, \\ C_z - \frac{1}{\sin \phi_2} < C_y. \end{cases} \quad (30)$$

For this case, the (29) or (30) is exactly the *sufficient and necessary condition* for non-vanishing intersectability of the given ray and voxel.

More precisely, by (27), if the  $i$  is given, the first two inequalities of (30) reads as the following inequality

$$C_1 - \tan \phi_1 - 1 < j < C_1. \quad (31)$$

Here

$$C_1 = \frac{N_y}{2} - s_1 \cos \phi_1 + s_2 \sin \phi_2 \sin \phi_1 - C_x \cos \phi_2 \sin \phi_1.$$

Fixed  $i$ , once we obtain the range of valid  $j$  by (31), the range of valid  $k$  can be calculated by the middle and last two inequalities of (30) as

$$\begin{cases} C_2 - \frac{\tan \phi_2}{\cos \phi_1} - 1 < k < C_2, \\ C_3 - 1 < k < C_3 + \frac{\tan \phi_2}{\sin \phi_1}. \end{cases} \quad (32)$$

Here

$$C_2 = \frac{N_z}{2} - s_2 \cos \phi_2 - C_x \sin \phi_2, \quad C_3 = \frac{N_z}{2} - s_2 \cos \phi_2 - C_y \sin \phi_2.$$

Hence for any given  $i$ , we can calculate the range of valid  $j$  by (31), and further that of  $k$  by the two inequalities in (32), to obtain those voxels intersecting with the given ray non-vanishingly. Similarly, provided that the  $j$  or  $k$  is given, the valid range of  $i$ ,  $k$  or  $i$ ,  $j$  can be calculated by the same method above. For those voxels, the condition (29) is definitely fulfilled. By merging the intervals in (28), the intersection reads as

$$C_{low} \leq t \leq C_{up}. \quad (33)$$

Otherwise, the intersection is empty. Hence, the *analytic formula* of the intersection length would be

$$l_{kji}(s_1, s_2, \phi_1, \phi_2) = \max(0, C_{up} - C_{low}). \quad (34)$$

*Remark 2.* For other similar cases, such as  $(\phi_1, \phi_2) \in \{(\pi/2, \pi) \cup (\pi, 3\pi/2) \cup (3\pi/2, 2\pi)\} \times (0, \pi/2)$ , the corresponding sufficient and necessary condition for non-vanishing intersectability, and analytic formula of the intersection length can be easily obtained by making quite minor changes for the derivation above. So we skip these negligible derivations.

**Case 2:**  $(\phi_1, \phi_2) = \{0\} \times (0, \pi/2)$ . Using simple computations, the condition (26) is translated into

$$\begin{cases} C_x \leq t \leq C_x + \frac{1}{\cos \phi_2}, \\ \frac{N_y}{2} - s_1 - 1 \leq t \leq \frac{N_y}{2} - s_1, \\ C_z - \frac{1}{\sin \phi_2} \leq t \leq C_z. \end{cases} \quad (35)$$

Here

$$\begin{cases} C_x = \frac{i - N_x/2 + s_2 \sin \phi_2}{\cos \phi_2}, \\ C_z = \frac{N_z/2 - k - s_2 \cos \phi_2}{\sin \phi_2}. \end{cases} \quad (36)$$

Following the derivation in **case 1** of this section, if all the valid  $j$  are outside the interval  $\frac{N_y}{2} - s_1 - 1 \leq j \leq \frac{N_y}{2} - s_1$ , or the first and last intervals in (35) have no overlap or their overlap is only a point, the length of the intersection is absolutely vanishing. To exclude this possibility, if and only if

$$\begin{cases} C_{low} < C_{up}, \\ \frac{N_y}{2} - s_1 - 1 \leq j \leq \frac{N_y}{2} - s_1. \end{cases} \quad (37)$$

Here

$$C_{low} = \max(C_x, C_z - 1/\sin \phi_2), \quad C_{up} = \min(C_x + 1/\cos \phi_2, C_z).$$

The (37) is equivalent to

$$\begin{cases} C_x < C_z, \\ C_z - \frac{1}{\sin \phi_2} < C_x + \frac{1}{\cos \phi_2}, \\ \frac{N_y}{2} - s_1 - 1 \leq j \leq \frac{N_y}{2} - s_1. \end{cases} \quad (38)$$

For this case, the (37) or (38) is the *sufficient and necessary condition* for non-vanishing intersectability of the given ray and voxel.

Moreover, by (36), if the  $i$  is given, the first two inequalities of (38) becomes the following inequality

$$C_1 - \tan \phi_2 - 1 < k < C_1. \quad (39)$$

Here

$$C_1 = \frac{N_z}{2} - s_2 \cos \phi_2 - C_x \sin \phi_2.$$

If the valid  $j$  satisfies  $\frac{N_y}{2} - s_1 - 1 \leq j \leq \frac{N_y}{2} - s_1$ , for given  $i$ , we can calculate the range of valid  $k$  by (39), to obtain those voxels intersecting with the given ray non-vanishingly. The *analytic formula* of the intersection length would be

$$l_{kji}(s_1, s_2, \phi_1, \phi_2) = \max(0, C_{up} - C_{low}). \quad (40)$$

*Remark 3.* For such cases  $(\phi_1, \phi_2) = \{\pi/2, \pi, 3\pi/2\} \times (0, \pi/2)$ , the sufficient and necessary condition for non-vanishing intersectability, and analytic formula of the intersection length can be immediately computed following the method in this case. So the trivial derivations are omitted here. Note that the rays in such cases are actually parallel to a certain coordinate plane, which leads the corresponding problem reduce to a 2D problem as derived above. However, the ambiguity perhaps happen (see the third example in section 4.1).

**Case 3:**  $(\phi_1, \phi_2) = (0, 0)$ . With simple calculations, the condition (26) reads as

$$\begin{cases} i - \frac{N_x}{2} \leq t \leq i - \frac{N_x}{2} + 1, \\ \frac{N_y}{2} - j - 1 \leq s_1 \leq \frac{N_y}{2} - j, \\ \frac{N_z}{2} - k - 1 \leq s_2 \leq \frac{N_z}{2} - k. \end{cases} \quad (41)$$

Evidently, for any given  $i$ , if the valid  $j$  satisfies  $\frac{N_y}{2} - s_1 - 1 \leq j \leq \frac{N_y}{2} - s_1$ , and the valid  $k$  also satisfies  $\frac{N_z}{2} - s_2 - 1 \leq k \leq \frac{N_z}{2} - s_2$ , the intersection length is unity, otherwise, it is zero.

*Remark 4.* For the cases as  $(\phi_1, \phi_2) \in \{\{\pi/2, \pi, 3\pi/2\} \times \{0\}\} \cup \{(0, \pi/2)\}$ , the intersection length can be computed by the method of the case above. So we omit the details. Obviously, the rays in such cases are parallel to a certain axis, which results in quite simple calculations. But the ambiguity perhaps happen (see the second example in section 4.1).

Remarkably, the computational cost of the proposed algorithm is still  $O(N)$  for any given ray, and  $O(NM)$  for all rays even to 3D circumstance. Here  $N$  represents the size of the image being reconstructed along one axis, and  $M$  denotes the number of rays. Hence, this algorithm achieves the degree of optimality, and its computational cost is optimal.

### 3.2.2 Circular cone beam

As mentioned previously, the cone beam is a projection geometry that is often used in 3D circumstance. Next, we will generalize the algorithm to this situation.

**Equiangular circular cone beam.** The equiangular cone beam is an extension of the equiangular fan beam into 3D situation. Actually, any ray of the equiangular cone beam can be specified by the parameters  $(D, \phi'_1, \alpha, \beta)$ , as shown in fig. 6. The source locates at  $xOy$  plane. Here  $D > 0$  indicates the distance of source for X-rays from the origin,  $\phi'_1 \in [0, 2\pi)$  stands for the angle between the center line from the source to origin and the positive  $x$ -axis, and  $\alpha \in (-\pi/2, \pi/2)$  determines the signed angle between the projection of the ray on  $xOy$  plane and the center line, and  $\beta \in (-\pi/2, \pi/2)$  denotes the signed angle between the ray and its projection on  $xOy$  plane.

Once given the parameters  $(D, \phi'_1, \alpha, \beta)$ , we can convert them into the parameters used in 3D parallel beam by performing the simple transformation as the following

$$\begin{cases} \phi_1 = \phi'_1 + \alpha, \\ \phi_2 = \beta, \\ s_1 = D \sin \alpha, \\ s_2 = D \cos \alpha \sin \beta. \end{cases} \quad (42)$$

**Equispaced circular cone beam.** The equispaced circular cone beam can also be derived in a similar way. The only difference is that it locates the ray using two distances  $(t, h)$  rather than two angles  $(\alpha, \beta)$ , as shown in fig. 6. The two distances specify the coordinate position of the detector in the projection plane. In other words, the parameters for equispaced cone beam is  $(D, \phi'_1, t, h)$ . Similarly, we can convert them into the parameters in 3D parallel beam as

$$\begin{cases} \phi_1 = \phi'_1 + \alpha, \\ \phi_2 = \beta, \\ s_1 = D \sin \alpha, \\ s_2 = h \cos^2 \alpha \cos \beta. \end{cases} \quad (43)$$

Here

$$\alpha = \arctan \frac{t}{D}, \quad \beta = \arctan \left( \frac{h}{\sqrt{D^2 + t^2}} \right).$$

After transformation, the associated X-ray transform in circular cone beam can be readily computed by the algorithm developed in section 3.2.1.

### 3.2.3 Helical cone beam

Helical cone beam is actually a type of cone beam that swipes through the detected body while the travelling path of its X-ray source relative to a fixed point on the body is shaped like a helix, as shown in fig. 7. Hence the source would have an additional parameter, i.e., the signed vertical distance to the origin.

**Equiangular helical cone beam.** Here the parameters are  $(D, \phi'_1, \beta_1, \beta_2, H)$ , where  $H$  determines the signed vertical distance from source to origin. Since in

section 3.2.2 only  $s_2$  is related to this vertical distance, to obtain the transformation, we just need to modify the last formula in (42) as

$$s_2 = D \cos \alpha \sin \beta + H \cos \beta. \quad (44)$$

The other formulas are still unchanged.

**Equispaced helical cone beam.** Similarly, the parameters for this beam is  $(D, \phi'_1, t, h, H)$ . To obtain the conversion, we only change the last formula of (43) as

$$s_2 = h \cos^2 \alpha \cos \beta + H \cos \beta, \quad (45)$$

and maintain the other formulas.

After minor changes, the X-ray transform in helical cone beam can be computed by the algorithm developed in section 3.2.1.

## 4 Discussions

For the problem itself, the ambiguities would happen to some special situations. This is intrinsic to the computation of the X-ray transform. Here we will have a discussion, and give a solution in the proposed algorithm. And the adaptability and parallelization of the algorithm will be further discussed.

### 4.1 Ambiguities and solution

**Ambiguities.** For the kind of situations as **case 2** in section 2.2.1 and **case 3** in section 3.2.1, the given ray is parallel to a certain axis, and the calculation of intersection is quite simple. More precisely, the length of intersection is just unity if it is non-vanishing. Nevertheless, when the given ray is exactly overlapping with grid line in 2D/3D scenarios, the ambiguity would happen to the problem itself.

As an example in 2D situation, let  $N_x = N_y = 5$ , and take the ray  $(1.5, 0)$  (i.e.,  $s = 1.5, \phi = 0$ ). By simple computations, for any given  $i$ , the intersection length is unity if  $0 \leq j \leq 1$ . Obviously, the same one intersection can be attributed to the ray  $(1.5, 0)$  with two different pixels  $(0, i)$  and  $(1, i)$  for  $0 \leq i \leq 4$ , simultaneously, which results in ambiguity.

Another example is given in 3D case. Let  $N_x = N_y = N_z = 4$ , and consider the ray  $(1, 1, 0, 0)$  (i.e.,  $s_1 = 1, s_2 = 1, \phi_1 = 0, \phi_2 = 0$ ). For each  $i$ , if  $0 \leq j \leq 1$  and  $0 \leq k \leq 1$ , the intersection length is unity. That is to say, the only one intersection can be assigned to the ray  $(1, 1, 0, 0)$  with four different voxels  $(0, 0, i)$ ,  $(0, 1, i)$ ,  $(1, 0, i)$  and  $(1, 1, i)$  for  $0 \leq i \leq 3$  coincidentally, which also leads to the ambiguity.

The other ambiguity would occur when the given ray is accurately on the grid plane, which is a special situation as described in **case 2** for 3D circumstance. For instance, let  $N_x = N_y = N_z = 3$ , think about the ray  $(-0.5, \sqrt{2}, 0, \pi/4)$  (i.e.,  $s_1 = -0.5, s_2 = \sqrt{2}, \phi_1 = 0, \phi_2 = \pi/4$ ). By simple calculations, we found that  $1 \leq j \leq 2$ , and only for  $i = 0$ , there exists the valid  $k = 0$ , and the length of intersection is  $\sqrt{2}$ , which is consistent with the geometric observation. In other words, the only one intersection can be assigned to the ray  $(-0.5, \sqrt{2}, 0, \pi/4)$  with two different voxels  $(0, 1, 0)$  and  $(0, 2, 0)$  simultaneously, which produces the ambiguity.

**Solution.** If the ambiguities above appear, to get rid of them, we can always consistently take the pixel/voxel with bigger (or lower) 1D-form index (see fig. 3 and fig. 8) as the intersected unit with the given ray in the proposed algorithm. For the first example, that is the pixel  $(1, i)$ . Because the pixel/voxel index is independent of the coordinate system. In this way, for any ray overlapping with a grid line or being on a grid plane, the pixels/voxels on the same side of the ray would be chosen reasonably.

## 4.2 Adaptability

The proposed algorithm is entirely obtained by mathematical derivations, which needs not compute any intersection point of the ray and the grid lines or planes. It is worth noting that even if the center of the image is not at the origin of the imaging coordinate system, or the scales  $(d_x, d_y, d_z)$  of the pixel/voxel or the sizes  $(N_x, N_y, N_z)$  of the image are different from each other along associated axes, the algorithm can be derived by the same pipeline.

The algorithm is independent of the specific scanning geometry, and can output the projection matrix in sparse storage. Because its fundamental element is to compute the intersection length of a certain ray with the pixels/voxels non-vanishingly intersecting with it. The algorithm can be immediately extended to deal with the scanning geometry that the rays are random distributed. Hence, the algorithm can be customized freely according to the requirements of the users, and more scanning geometries can be easily added into the framework based on the proposed algorithm.

## 4.3 Parallelization

Since the proposed algorithm implements the calculation of intersection length ray by ray and unit by unit (pixel/voxel), it is quite suited to parallelize and the computational complexity per parallel thread achieves  $O(1)$ .

## 5 Validations

The algorithm proposed above has been validated through different test examples. Specific tests can be found as follows. This algorithm calculates the X-ray transform accurately using mathematical derivations, so there is no error. However, since the calculation is done in float data type and the program is written in C++ language, the result only has six significant digits. Since the scales of each unit (pixel/voxel) are fixed to be unity, the output is accurate down to around five decimal places, which should be accurate enough in most cases. If the higher precision is required, the program can calculate down to 15 decimal places by switching float data type into double data type. Due to the limitation of space, not all tests can be given here. Thus, we will give only one test for each scanning geometry. Although this is not a full evaluation, the tests illustrate the correctness of the proposed method.

### 5.1 Test suite 1: 2D parallel beam

In 2D circumstance, the first example is for 2D parallel beam. Assuming that the size of the image is  $3 \times 3$ . In this situation, one easy-to-understand example

is a ray with  $\pi/4$  angle to the positive  $x$ -axis and a distance of unity to the origin, namely, the ray  $(1, \pi/4)$ .

Using intuitively geometric computation, the valid intersections of the ray with all the pixels can be fast obtained, where the intersected pixels are  $(0, 0)$ ,  $(0, 1)$  and  $(1, 0)$ , and the corresponding intersection lengths are  $2 - \sqrt{2}$ ,  $2\sqrt{2} - 2$  and  $2\sqrt{2} - 2$ , respectively.

On the other hand, we compute the results by hand along the algorithm in section 2.2.1.

- (i) If  $i = 0$ , then  $C_x = -3\sqrt{2}/2 + 1$ ,  $C_1 = 3 - \sqrt{2}$ , and then the valid  $j$  includes 0 and 1. The  $C_y = 3\sqrt{2}/2 - 1$  and  $\sqrt{2}/2 - 1$  for  $j = 0$  and 1 respectively. Hence, the lengths of intersections of the ray with pixels  $(0, 0)$  and  $(1, 0)$  are  $2 - \sqrt{2}$  and  $2\sqrt{2} - 2$ , respectively;
- (ii) If  $i = 1$ , then  $C_x = -\sqrt{2}/2 + 1$ ,  $C_1 = 5/2 - 3\sqrt{2}/2$ , and the valid  $j$  only contains 0. So the  $C_y = 3\sqrt{2}/2 - 1$ . The length of intersection of the ray with pixel  $(0, 1)$  is  $2\sqrt{2} - 2$ ;
- (iii) If  $i = 2$ , the valid  $j$  is empty.

By numerical implementation, the output of the valid lengths of intersections is shown in table 1, with the first column being the 1D-form index of the pixel and the corresponding second column showing the intersection length. Keep in mind that the 1D-form index and the 2D-form one can be converted into each other.

0	0.585787
1	0.828427
3	0.828427

Tab. 1: Output of the example for 2D parallel beam

Obviously, the above results are completely consistent with each other if we do not consider the machine error.

## 5.2 Test suite 2: Fan beam

Here we only give an example for the equiangular fan beam because the validation has no essential distinction with that of the equispaced one. For equiangular fan beam, the main algorithm are the same as the 2D parallel beam. What we just need to do is to get the corresponding parameters  $(s, \phi)$  in 2D parallel beam for each ray when given  $(D, \alpha, \gamma)$ , as described in section 2.2.2.

As an example, the size of the image is assumed to be  $4 \times 4$ , the ray is considered with parameters  $D = 4$ ,  $\alpha = \pi/2$ ,  $\gamma = -\pi/6$ .

With (17), the parameters are transformed into the associated ones in 2D parallel beam as  $s = -2$ ,  $\phi = -\pi/6$ . As observed in section 2.2.1, it indicates the ray  $(2, 5\pi/6)$ .

By directly analytic geometry, the valid intersections of the ray with all the pixels can be gained immediately, where the intersected pixels are  $(3, 0)$  and  $(3, 1)$ , and the corresponding lengths of intersections are  $2\sqrt{3}/3$  and  $4 - 2\sqrt{3}$ , respectively.

Then we recompute the results by hand along the algorithm in section 2.2.1.

- (i) If  $i = 0$ , then  $C_x = 2\sqrt{3}/3$ , and then the valid  $j$  should satisfy  $1 + 2\sqrt{3}/3 < j < 2 + \sqrt{3}$ . Hence, the valid  $j$  only contains 3. The  $C_y = 2\sqrt{3} - 2$  for  $j = 3$ .

Hence, the length of intersection of the ray with pixels  $(3, 0)$  is  $2\sqrt{3}/3$ ;  
 (ii) If  $i = 1$ , then  $C_x = 0$ , and the valid  $j$  should satisfy  $1 + \sqrt{3} < j < 2 + 4\sqrt{3}/3$ . So the valid  $j$  only contains 3. Then  $C_y = 2\sqrt{3} - 2$  as well. The length of intersection of the ray with pixel  $(3, 1)$  is  $4 - 2\sqrt{3}$ ;  
 (iii) If  $i = 2$  or 3, the valid  $j$  is empty.

By numerical implementation, the output of the valid lengths of intersections is shown in table 2. The 12th and 13th pixels in 1D form are the pixels  $(3, 0)$  and  $(3, 1)$ , respectively.

12	1.1547
13	0.535899

Tab. 2: Output of the example for equiangular fan beam

It is easy to observe that the above results are completely consistent with each other if we do not take care the machine error.

### 5.3 Test suite 3: 3D parallel beam

In 3D situation, we first consider the 3D parallel beam. Assuming that the size of the image is  $3 \times 3$ . In this case, one intuitive example is a ray with  $\pi/4$  angle to both the positive  $x$ - and  $y$ -axis and a distance of zero to the origin, namely, the ray  $(0, 0, \pi/4, \pi/4)$ .

Not that the given ray locates at one diagonal plane of the image. We can immediately calculate out the valid intersections of the ray with all the voxels by geometric observation. The valid intersected voxels are  $(0, 0, 2)$ ,  $(0, 1, 1)$ ,  $(1, 1, 1)$ ,  $(2, 1, 1)$  and  $(2, 2, 0)$ , and the corresponding lengths of intersections are  $3\sqrt{2}/2 - 1$ ,  $1 - \sqrt{2}/2$ ,  $\sqrt{2}$ ,  $1 - \sqrt{2}/2$  and  $3\sqrt{2}/2 - 1$ , respectively.

Then we recompute the results by hand along the algorithm in section 3.2.1.  
 (i) If  $i = 0$ , then  $C_x = -3$ , and then the valid  $j$  should satisfy  $1 < j < 3$ . Hence, the valid  $j$  only contains 2. The  $C_y = -1$  for  $j = 2$ . Then the valid  $k$  should satisfy  $(1 + \sqrt{2})/2 < k < (3 + 3\sqrt{2})/2$ . So the valid  $k$  includes only 2. Hence, the length of intersection of the ray with pixels  $(2, 2, 0)$  is  $3\sqrt{2}/2 - 1$ ;  
 (ii) If  $i = 1$ , then  $C_x = -1$ , and the valid  $j$  should satisfy  $0 < j < 2$ . So the valid  $j$  only contains 1. Then  $C_y = 1$  for  $j = 1$ . Then the valid  $k$  should satisfy  $(1 - \sqrt{2})/2 < k < (3 + \sqrt{2})/2$ . So the valid  $k$  includes 0, 1, and 2. The lengths of intersections of the ray with voxels  $(0, 1, 1)$ ,  $(1, 1, 1)$  and  $(2, 1, 1)$  are  $1 - \sqrt{2}/2$ ,  $\sqrt{2}$ , and  $1 - \sqrt{2}/2$ , respectively;  
 (iii) If  $i = 2$ , then  $C_x = 1$ , and then the valid  $j$  should satisfy  $-1 < j < 1$ . Hence, the valid  $j$  only contains 0. The  $C_y = 3$  for  $j = 0$ . Then the valid  $k$  should satisfy  $(1 - 3\sqrt{2})/2 < k < (3 - \sqrt{2})/2$ . So the valid  $k$  includes only 0. Hence, the length of intersection of the ray with pixels  $(0, 0, 2)$  is  $3\sqrt{2}/2 - 1$ .

By numerical implementation, the output of the valid lengths of intersections is shown in table 3. The 2nd, 4th, 13th, 22nd and 24th voxles in 1D form are the voxels  $(0, 0, 2)$ ,  $(0, 1, 1)$ ,  $(1, 1, 1)$ ,  $(2, 1, 1)$  and  $(2, 2, 0)$ , respectively.

Evidently, the above results are completely consistent with each other if we neglect the machine error.

2	1.12132
4	0.292893
13	1.41421
22	0.292893
24	1.12132

Tab. 3: Output of the example for 3D parallel beam

#### 5.4 Test suite 4: Circular cone beam

Since the validation of equispaced circular cone beam has no essential distinction with that of the equiangular one, here we just give an example for the equiangular case.

As an example, the size of the image is assumed to be  $4 \times 4$ , the given ray is assigned with parameters  $D = 4$ ,  $\phi'_1 = \pi/4$ ,  $\alpha = \pi/12$ , and  $\beta = \pi/12$ . Transforming these parameters into the associated ones in 3D parallel beam by (42), we have  $\phi_1 = \pi/3$ ,  $\phi_2 = \pi/12$ ,  $s_1 = 4 \sin(\pi/12)$ ,  $s_2 = 4 \sin(\pi/12) \cos(\pi/12)$ .

For this example, the main algorithm are almost the same as the 3D parallel beam. So we neglect the calculations by hand following the algorithm in section 3.2.2 as the test above.

Using solid geometry, we can analytically calculate out the valid intersections of the ray with all the voxels. We list the valid intersected voxels and the corresponding lengths of intersections as follows

$$\begin{aligned}
 \text{voxel } (1, 3, 0) : & 2(1 - (4 - \sqrt{2}) \tan(\pi/12) \sin(5\pi/12) / \sin(\pi/3)) / \cos(\pi/12); \\
 \text{voxel } (1, 2, 0) : & 2\sqrt{3} / (3 \cos(\pi/12)); \\
 \text{voxel } (1, 1, 0) : & 2((4 - \sqrt{2}) \tan(\pi/12) \sin(5\pi/12) / \sin(\pi/3) - \sqrt{3}/3) / \cos(\pi/12); \\
 \text{voxel } (0, 0, 1) : & 2\sqrt{3} / (3 \cos(\pi/12)); \\
 \text{voxel } (1, 1, 1) : & (1 - (4\sqrt{2} - 2) \tan(\pi/12)) / \sin(\pi/12); \\
 \text{voxel } (0, 1, 1) : & (((4 - \sqrt{2})(\sqrt{2} - 2 \tan(\pi/12) \sin(5\pi/12) / \sin(\pi/3)) \\
 & + 4\sqrt{3}/3) \tan(\pi/12) - 1) / \sin(\pi/12).
 \end{aligned}$$

By numerical implementation, the output of the valid lengths of intersections is shown in table 4. The 1st, 5th, 20th, 21st, 24th and 28th voxels in 1D form are the voxels  $(0, 0, 1)$ ,  $(0, 1, 1)$ ,  $(1, 1, 0)$ ,  $(1, 1, 1)$ ,  $(1, 2, 0)$  and  $(1, 3, 0)$ , respectively.

1	1.19543
5	0.712929
20	0.404656
21	0.0778492
24	1.19543
28	0.470462

Tab. 4: Output of the example for equiangular circular cone beam

As we have checked up, the above results are completely consistent with each other if we neglect the machine error.

### 5.5 Test suite 5: Helical cone beam

Here we just give an example for the equiangular helical cone beam. The geometry of this case is almost the same as the equiangular circular cone beam except with one more signed vertical distance.

When we choose the vertical distance  $H = 0$ , and maintain those parameters in section 5.4, as expected, the output of the numerical implementation is the same as the corresponding equiangular circular cone beam.

In contrast, we take  $H = 0.5$ . Transforming these parameters into the associated ones in 3D parallel beam by (42) and (44), we have  $\phi_1 = \pi/3$ ,  $\phi_2 = \pi/12$ ,  $s_1 = 4 \sin(\pi/12)$ ,  $s_2 = 4 \cos(\pi/12) \sin(\pi/12) + \cos(\pi/12)/2$ .

Similarly, we can analytically calculate out the valid intersections of the ray with all the voxels. The results of valid intersected voxels and the corresponding lengths of intersections are listed as follows

$$\begin{aligned}
 & \text{voxel } (0, 2, 0) : 2\sqrt{3}/(3 \cos(\pi/12)); \\
 & \text{voxel } (0, 1, 0) : 2((4 - \sqrt{2}) \tan(\pi/12) \sin(5\pi/12) / \sin(\pi/3) - \sqrt{3}/3) / \cos(\pi/12); \\
 & \text{voxel } (0, 0, 1) : 2\sqrt{3}/(3 \cos(\pi/12)); \\
 & \text{voxel } (0, 1, 1) : (2 - (8 - 2\sqrt{2}) \tan(\pi/12) \sin(5\pi/12)) / (\cos(\pi/6) \cos(\pi/12)); \\
 & \text{voxel } (0, 3, 0) : (0.5 - (4\sqrt{2} - 4) \tan(\pi/12)) / \sin(\pi/12); \\
 & \text{voxel } (1, 3, 0) : 2(1 - (4 - \sqrt{2}) \tan(\pi/12) \sin(5\pi/12) / \sin(\pi/3)) / \cos(\pi/12) \\
 & \quad - (0.5 - (4\sqrt{2} - 4) \tan(\pi/12)) / \sin(\pi/12).
 \end{aligned}$$

Furthermore, the output of the numerical implementation is given in table 5. The 1st, 4th, 5th, 8th, 12th and 28th voxels in 1D form corresponds to the voxels  $(0, 0, 1)$ ,  $(0, 1, 0)$ ,  $(0, 1, 1)$ ,  $(0, 2, 0)$ ,  $(0, 3, 0)$  and  $(1, 3, 0)$ , respectively.

1	1.19543
4	0.404656
5	0.790778
8	1.19543
12	0.253912
28	0.21655

Tab. 5: Output of the example for equiangular helical cone beam

For this example, it is easy to validate that the analytic results and the corresponding numerical ones are also completely consistent with each other if the machine error is neglected.

## 6 Conclusions

A fast, accurate, adaptive and parallelizable algorithm has been proposed to compute the X-ray transform of an image represented by unit (pixel/voxel) basis functions, for various 2D/3D scanning geometries, such as 2D/3D parallel beam, 2D fan beam, 3D circular/helical cone beam, etc. The algorithm can

be used to assist implementing the iterative or deep learning based reconstruction algorithms for various tomographic imaging arisen in medicine, biology, industry, and so on.

More importantly, the sufficient and necessary condition is derived for non-vanishing intersectability, and the analytic formula is also obtained for the intersection length, which can be used to distinguish the units that produce valid intersections with the given ray, and then perform simple calculations only for those units. Based on the results above, the algorithm becomes quite easy to be implemented, and the amount of computations are significantly reduced. Its computational cost is  $O(N)$  for any given ray, and  $O(NM)$  for all rays, to both 2D and 3D circumstance. Here the  $N$  represents the size of the image being reconstructed along one axis, and  $M$  denotes the number of rays. Hence, the computational complexity of this algorithm is optimal.

To the problem itself, we further discussed the intrinsic ambiguities that perhaps happen, and have presented a solution in the algorithm. Moreover, the algorithm not only possesses the adaptability with regard to the center position, scale and size of the image, and the scanning geometry as well, but also is quite suited to parallelize with optimality. The projection matrix can be sparsely stored and output if needed, and the adjoint of X-ray transform can be also computed by the algorithm. Hence, the algorithm can be customized freely according to the requirements of the user, and more scanning geometries can be easily added into the framework based on the proposed algorithm.

The correctness of the proposed algorithm has been validated by several test examples for various scanning geometries. For each scanning geometry, we provided one test suite. As the pipeline, we first calculated the analytic results by solid geometry, and/or recomputed the results by hand along the proposed algorithm, which construct the standard references being used to make comparisons. And then we computed the associated numerical results by numerical implementation. As demonstrated by these compared results, the proposed algorithm can yield precise results for various scanning geometries.

## References

- [1] J. Adler and O. Öktem. Solving ill-posed inverse problems using iterative deep neural networks. *Inverse Problems*, 33(12):124007, 2017.
- [2] S. Arridge, P. Maass, O. Öktem, and C.-B. Schönlieb. Solving inverse problems using data-driven models. *Acta Numer.*, 28:1–174, 2019.
- [3] A. Biguri, M. Dosanjh, S. Hancock, and M. Soleimani. TIGRE: a MATLAB-GPU toolbox for CBCT image reconstruction. *Biomed. Phys. Eng. Express*, 2(5):055010, 2016.
- [4] P. Charbonnier, L. Blanc-Féraud, G. Aubert, and M. Barlaud. Deterministic edge-preserving regularization in computed imaging. *IEEE Transactions on Image Processing*, 6(2):298–311, 1997.
- [5] C. Chen, B. Gris, and O. Öktem. A New Variational Model for Joint Image Reconstruction and Motion Estimation in Spatiotemporal Imaging. *SIAM Journal on Imaging Sciences*, 12(4):1686–1719, 2019.

- [6] C. Chen and G. Xu. A new linearized split Bregman iterative algorithm for image reconstruction in sparse-view X-ray computed tomography. *Computers and Mathematics with Applications*, 71(8):1537–1559, 2016.
- [7] S. R. Cherry, J. A. Sorenson, and M. E. Phelps. *Physics in nuclear medicine*. Elsevier, fourth edition, 2012.
- [8] B. De Man and S. Basu. Distance-driven projection and backprojection in three dimensions. *Phys. Med. Biol.*, 49:2463–2475, 2004.
- [9] A. H. Delaney and Y. Bresler. Globally convergent edge-preserving regularized reconstruction: an application to limited-angle tomography. *IEEE Transactions on Image Processing*, 7(2):204–221, 1998.
- [10] B. Dong, J. Li, and Z. Shen. X-ray CT image reconstruction via wavelet frame based regularization and Radon domain inpainting. *J. Sci. Comput.*, 54(2-3):333–349, 2013.
- [11] J. Frank. *Electron tomography: methods for three-dimensional visualization of structures in the cell*. Springer Verlag, 2006.
- [12] J. Frank. *Three-dimensional electron microscopy of macromolecular assemblies: visualization of biological molecules in their native state*. Oxford University Press, 2006.
- [13] H. Gao. Fast parallel algorithms for the x-ray transform and its adjoint. *Medical Physics*, 39(11):7110–7120, 2012.
- [14] H. Gupta, K. H. Jin, H. Q. Nguyen, M. T. McCann, and M. Unser. CNN-Based Projected Gradient Descent for Consistent CT Image Reconstruction. *IEEE Transactions on Medical Imaging*, 37(6):1440–1453, 2018.
- [15] G. Han, Z. Liang, and J. You. A Fast Ray-Tracing Techniques for TCT and ECT Studies. In *Proceedings of the IEEE Nuclear Science Symposium and Medical Imaging Conference*, pages 1515–1518, 1999.
- [16] S. Helgason. *The Radon transform*. Birkhäuser, Boston, second edition, 1999.
- [17] J. Hsieh. *Computed tomography: principles, design, artifacts, and recent advances*. SPIE Press, second edition, 2009.
- [18] J. Hsieh, B. Nett, Z. Yu, K. Sauer, J. Thibault, and C. Bouman. Recent advances in CT image reconstruction. *Current Radiology Reports*, 1(1):39–51, 2013.
- [19] F. Jacobs, E. Sundermann, B. De Sutter, M. Christiaens, and I. Lemahieu. A Fast Algorithm to Calculate the Exact Radiological Path through a Pixel or Voxel Space. *Journal of computing and information technology*, 6(1):89–94, 1998.
- [20] M. Jiang and G. Wang. Convergence studies on iterative algorithms for image reconstruction. *IEEE Transactions on Medical Imaging*, 22(5):569–579, 2003.

- [21] A. C. Kak and M. Slaney. *Principles of Computerized Tomographic Imaging*. SIAM, Philadelphia, 2001.
- [22] M. Li, G. Xu, C. O. S. Sorzano, F. Sun, and C. L. Bajaj. Single-particle reconstruction using L2-gradient flow. *Journal of Structural Biology*, 176:259–267, 2011.
- [23] J. Liu, X. Zhang, H. Zhao, Y. Gao, D. Thomas, D. Low, and H. Gao. 5D respiratory motion model based image reconstruction algorithm for 4D cone-beam computed tomography. *Inverse Problems*, 31:115007, 2015.
- [24] R. Liu, L. Fu, B. De Man, and H. Yu. GPU-Based Branchless Distance-Driven Projection and Backprojection. *IEEE Transactions on Computational Imaging*, 3(4):617–632, 2017.
- [25] Y. Long, J. M. Fessler, and M. Balter. 3-D forward and back-projection for x-ray CT using separable footprints. *IEEE Trans. Med. Imaging*, 29:1839–1850, 2010.
- [26] F. Natterer. The mathematics of computerized tomography (classics in applied mathematics, vol. 32). *Inverse Problems*, 18:283–284, 2001.
- [27] S. Ramani and J. Fessler. A splitting-based iterative algorithm for accelerated statistical X-ray CT reconstruction. *IEEE Transactions on Medical Imaging*, 31(3):677–688, 2012.
- [28] S. Rit, M. Vila Oliva, S. Brousmiche, R. Labarbe, D. Sarrut, and G. C. Shar. The reconstruction toolkit (RTK), an open-source cone-beam CT reconstruction toolkit based on the insight toolkit (ITK). *Journal of Physics: Conference Series*, 489:012079, 2014.
- [29] C. Shen, Y. Gonzalez, L. Chen, S. B. Jiang, and X. Jia. Intelligent Parameter Tuning in Optimization-Based Iterative CT Reconstruction via Deep Reinforcement Learning. *IEEE Transactions on Medical Imaging*, 37(6):1430–1439, 2018.
- [30] R. L. Siddon. Fast calculation of the exact radiological path for a three-dimensional ct array. *Medical Physics*, 12(2):252–255, 1985.
- [31] E. Sidky, J. Jørgensen, and X. Pan. Convex optimization problem prototyping for image reconstruction in computed tomography with the Chambolle–Pock algorithm. *Physics in Medicine and Biology*, 57(10):3065, 2012.
- [32] E. Sidky, C. Kao, and X. Pan. Accurate image reconstruction from few-views and limited-angle data in divergent-beam CT. *Journal of X-ray Science and Technology*, 14(2):119–139, 2006.
- [33] J. Thibault, K. Sauer, C. Bouman, and J. Hsieh. A three-dimensional statistical approach to improved image quality for multislice helical CT. *Medical physics*, 34(11):4526–4544, 2007.
- [34] K. Thielemans, C. Tsoumpas, S. Mustafovic, T. Beisel, P. Aguiar, N. Dikaios, and M. W. Jacobson. STIR: Software for Tomographic Image Reconstruction Release 2. *Physics in Medicine and Biology*, 57(4):867–883, 2012.

- [35] W. van Aarle, W. J. Palenstijn, J. Cant, E. Janssens, F. Bleichrodt, A. Dabravolski, J. De Beenhouwer, K. J. Batenburg, and J. Sijbers. Fast and Flexible X-ray Tomography Using the ASTRA Toolbox. *Optics Express*, 24(22):25129–25147, 2016.
- [36] G. Xu and C. Chen. Blended finite element method and its convergence for three-dimensional image reconstruction using  $l^2$ -gradient flow. *Commun. Math. Sci.*, 12(6):989–1015, 2014.
- [37] B. Yang, L. Ying, and J. Tang. Artificial Neural Network Enhanced Bayesian PET Image Reconstruction. *IEEE Transactions on Medical Imaging*, 37(6):1297–1309, 2018.
- [38] H. Zhao and A. J. Reader. Fast ray-tracing technique to calculate line integral paths in voxel arrays. In *Proceedings of the IEEE Nuclear Science Symposium and Medical Imaging Conference*, pages 2808–2812, 2003.